The influence of fluid-sensitive dispersion and attenuation on AVO analysis

Geophys. J. Int. (2006) **167,** 89–105 doi: 10.1111/j.1365-246X.2006.02919.x

The influence of fluid-sensitive dispersion and attenuation on AVO analysis

Mark Chapman, Enru Liu and Xiang-Yang Li

Edinburgh Anisotropy Project, British Geological Survey, Murchison House, West Mains Road, Edinburgh, EH9 3LA, *UK. E-mail: m.chapman@bgs.ac.uk*

Accepted 2006 January 17. Received 2005 October 11; in original form 2005 June 8

SUMMARY

Analysis of seismic data suggests that hydrocarbon deposits are often associated with higher than usual values of attenuation, but this is generally ignored during amplitude-versus-offset (AVO) analysis. The effect can be modelled with equivalent medium theory based on the squirt flow concept, but the excess attenuation is associated with strong velocity dispersion. Consequently, when we study reflections from the interface between such an equivalent medium and an elastic overburden we find that the reflection coefficient varies with frequency. The impact of this variation depends on the AVO behaviour at the interface; class I reflections tend to be shifted to higher frequency while class III reflections have their lower frequencies amplified. We calculate synthetic seismograms for typical models using the reflectivity method for materials with frequency dependent velocities and attenuations, and find that these effects are predicted to be detectable on stacked data. Two field data sets show frequency anomalies similar to those predicted by the analysis, and we suggest that our modelling provides a plausible explanation of the observations.

Key words: amplitude-versus-offset, attenuation, dispersion, hydrocarbons.

INTRODUCTION

Seismic 'low-frequency effects' have been noted with reference to reflections from hydrocarbon-saturated rocks for many years (Taner *et al.* 1979), but recently there has been an upsurge in interest in the topic (van der Kolk *et al.* 2001; Castagna *et al.* 2003; Korneev *et al.* 2004; Ebrom 2004; Holzner *et al.* 2005). Much of this interest has been driven by the increasing success of modern spectral decomposition methods (Burnett *et al.* 2003), which render the frequency dependent character of the reflections particularly clear. Nevertheless, it is not clear whether these observations represent the true earth response or whether they have been induced by processing methods (Ebrom 2004).

What does appear clear is that direct quality factor (Q) measurements indicate that hydrocarbon-saturated zones often show anomalously high values of attenuation (Castagna *et al.* 1993; Klimentos 1995; Dasios *et al.* 2001; Dasgupta & Clark 1998; Rapoport *et al.* 2004; Maultzsch *et al.* 2003), although low Q zones can also be associated with fracturing (Worthington & Hudson 2000). While Q is considered to be frequency dependent over a wide frequency band (Sams *et al.* 1997), it is unclear whether the frequency dependence of Q can be observed in band limited seismic data (Harris *et al.* 1997). It is in general to be expected that strong attenuation should be associated with significant velocity dispersion.

Nevertheless, and despite some promising attempts to consider systematic frequency variations with offset (Mazzotti 1991; Shen *et al.* 2002), standard amplitude-versus-offset (AVO) analysis typically ignores attenuation, making use of purely elastic reflectivity modelling. Some effort has gone into correcting for the effect of attenuation in the overburden (Luh 1993; Carcione *et al.* 1998; Carcione 1999) with the ultimate goal of equalizing the frequency content in the near and far stacks, but the excess reservoir attenuation has received rather less attention.

Much of this neglect can perhaps be explained by the natural desire to discuss poroelastic effects within the framework of the Biot theory (Biot 1956). Unfortunately, the Biot theory greatly underestimates the measured attenuation (Mavko *et al.* 1998); it predicts negligible attenuation at seismic frequencies (Dutta & Ode 1983) and local flow mechanisms are typically invoked to account for observed dispersion and attenuation in the interpretation of laboratory measurements (Mavko & Jizba 1991; Best *et al.* 1994; Assefa *et al.* 1999; King & Marsden 2002). Higher values of attenuation can, however be obtained when we consider heterogeneous media (Gurevich *et al.* 1997; Carcione 1998).

Many authors have used Biot's theory to study the generation of reflected and transmitted waves at the interface between poroelastic layers with different fluid saturations (Geertsma & Smit 1961; Deresiewicz & Rice 1964; Dutta & Ode 1983; Pride *et al.* 2002; Denneman *et al.* 2002; Gurevich & Schoenberg 1999; Gurevich *et al.* 2004; Bourbie *et al.* 1987), with the main point of difference to the elastic case being the propensity of the incident P wave to generate a 'slow' Biot wave at the interface. The Biot wave has been observed in Nievelsteiner sandstone, which has exceptionally high values of porosity and permeability (Kelder & Smeulders 1997), but

more generally the Biot wave is not observed in real rocks (Klimentos & McCann 1988).

If we confine our interest to the reflection coefficient for a single interface then, with some notable exceptions (Denneman *et al.* 2002), the conclusion of these studies is that for typical rock properties of interest the theory predicts behaviour which does not materially differ from the elastic case at seismic frequencies (Dutta & Ode 1983; Gurevich 1996). Thus it has not so far proven possible to address observed frequency effects in the framework of the standard Biot model (Goloshubin & Bakulin 1998). The potentially valuable interpretation of such frequency effects has, therefore, been hampered.

Our interpretation is that this failure arises from the inability of the Biot model to account for observed values of attenuation. Efforts are underway to develop Biot's ideas to account for observed attenuation at seismic frequencies (Pride *et al.* 2004), typically by introducing heterogeneities with significant scale lengths. In future it may be possible to address this problem with a truly satisfactory, mathematically rigorous, model based on Biot's theory.

The philosophy, which we wish to develop in this paper holds that abnormally high reservoir attenuation is the observed ground truth, and we should, therefore, concentrate our attention on those physical mechanisms which can explain the existence of the excess attenuation associated with the hydrocarbon deposit. Two related, but distinct, mechanisms appear to us to be likely candidates; scattering due to increased heterogeneity in hydrocarbon-saturated rocks, and fluid flow.

Wave propagation in a layered medium can be described both by the Backus average (Backus 1962) of equivalent medium theory and the familiar ray theory. The Backus average assumes long wavelength (low frequency) while ray theory is a high-frequency approximation. In intermediate cases we see dispersion and apparent attenuation (O'Doherty & Anstey 1971; Shapiro & Zien 1993; Marion *et al.* 1994; Werner & Shapiro 1998; van der Baan 2001). The magnitude of the apparent attenuation often increases as the low- and high-frequency limits move further apart. Liu (2004) has argued in the context of gas detection that the introduction of hydrocarbons causes increased heterogeneity, moving the ray and Backus averages apart and that this gives rise to increased attenuation. Dvorkin & Uden (2004) have considered a similar effect relevant to gas hydrate saturation and have argued that its influence is almost comparable to the fluid induced losses. We consider this to be a very strong candidate mechanism for the increase of attenuation in gas-saturated zones.

The alternative approach is based on the assumption that fluid-flow phenomena are responsible for the increased attenuation. White (1975) and Dutta & Ode (1979) considered the case in which gas 'bubbles' are present in otherwise fluid-saturated rock and showed that the deformation of the bubbles by the passing seismic waves gives rise to a powerful attenuation and dispersion mechanism. A key role is played by the size of the bubbles and the percentage of gas saturation. This analysis has been extended by Carcione *et al.* (2003).

In parallel to these developments a range of papers, beginning with Mavko & Nur (1975), have advanced models of the 'squirt-flow' mechanism. Such models consider that a passing seismic wave gives rise to unequal pore-fluid pressures in different parts of the pore space, and that the resulting pressure gradients relax on a particular timescale. When the seismic wave frequency is comparable to the inverse of the timescale parameter, substantial dispersion and attenuation are known to occur. The interest in the theory is driven by two factors; the magnitude of the predicted attenuation is much higher than that associated with the traditional Biot mechanisms and the characteristic frequency varies directly with permeability and inversely with viscosity. Such a dependence of the characteristic frequency is opposite to that of the Biot theory, and it is generally easier to reconcile laboratory measurements with such a relationship than with the standard Biot model (Batzle *et al.* 2001). Sometimes (Mavko & Jizba 1991; Pride *et al.* 2004) the term 'squirt flow' is used with the connotation that the fluid dynamics take place at the grain scale only. Our preference is to define 'squirt flow' as being a mechanism whose characteristic frequency is proportional to the ratio of permeability to fluid viscosity, and so include a range of meso-scale fluid processes in the discussion. When we consider only grain-scale processes the transition frequency is generally above the seismic band, but the consideration of inhomogeneities on larger scales can move the transition frequency downwards, and thus provide a plausible mechanism for attenuation at seismic frequencies (Chapman 2003).

Our modelling follows the philosophy of Le Ravalec & Gueguen (1996) and Endres & Knight (1997). This approach is based on inclusion models derived ultimately from the formulae of Eshelby (1957). The low-frequency limits are calculated by Gassmann-saturating the elastic tensor, which comes from equivalent medium theory with empty inclusions, and this corresponds to the case of pressure equalization. A high-frequency limit is defined in terms of the standard equivalent medium model with inclusions whose elastic properties are those of the fluid. The dispersion is calculated as the difference between the low- and high-frequency limits.

A limitation of these calculations is the inability to calculate attenuation directly. Chapman *et al.* (2002) developed a model for the time-dependent relaxation of wave-induced pressure gradients in an isotropic rock whose pore space consisted of spherical pores and randomly oriented thin ellipsoidal cracks, based on nearest neighbour exchange of fluid in response to grain-scale pressure gradients. The solution of this model was incorporated into equivalent medium calculations based on those of Eshelby (1957) to allow the computation of a complex valued effective elastic tensor in the frequency domain. From these results we can replace the fluid-saturated composite material with a homogeneous material with specified velocity and attenuation at each frequency. This analysis was extended to the anisotropic, multiscale case by Chapman (2003). The model is Gassmann consistent at low frequency and reduces to the standard equivalent medium theory at high frequency, implying that we have interpolated between the two, purely elastic, limits described by Le Ravalec & Gueguen (1996) and Endres & Knight (1997). The mathematical description of the model is set out in the Appendix.

Fig. 1 illustrates the predicted dependence of *P*-wave attenuation on fluid bulk modulus (normalized by the bulk modulus of water) for a range of inclusion (crack) aspect ratios. Note that in this notation, hydrocarbons will typically have normalized bulk moduli around 10^{-1} to 10^{-2} (Batzle & Wang 1992), while air at room temperature, the value appropriate for many 'dry rock' laboratory experiments, typically has a normalized bulk modulus around 7×10^{-5}.

Fig. 1 demonstrates that attenuation is negligible for both low and high limiting values of the fluid bulk modulus. This makes sense since if the fluid were supposed to have the same elastic properties as the rock matrix we would expect to return to an homogeneous elastic material, but if the fluid bulk modulus were zero we would return to a dry rock, for which the model incorporates no attenuation mechanism. Note that the peak in attenuation tends to occur for typical hydrocarbon values. This emphasizes again the need to differentiate between 'dry' and 'gas-saturated' conditions (Mavko *et al.* 1998). Although there is substantial dependence of the behaviour on the

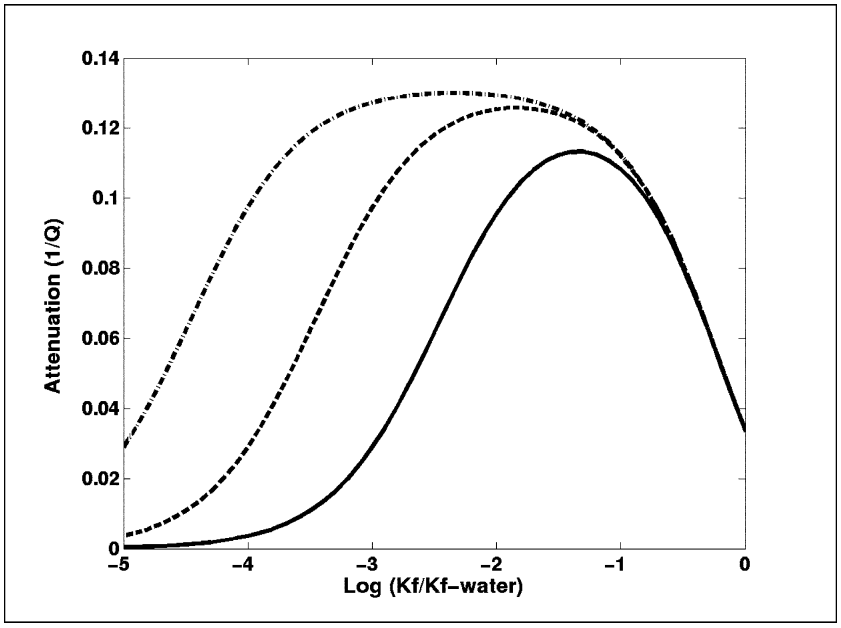

Figure 1. *P*-wave attenuation as a function of normalized fluid bulk modulus, for Model 1. Propagation is at the characteristic frequency $\omega\tau = 1$ and we assume aspect ratios of 10^{-3} (solid line), 10^{-4} (dashed line) and 10^{-5} (dotted-dashed line).

aspect ratio, this occurs for low fluid bulk moduli; for values typical of water or hydrocarbons there is only a weak dependence on the aspect ratio. Consequently, in the remainder of the paper we will assume an aspect ratio of 10^{-3} for the purposes of performing the calculations and implicitly suppress aspect ratio dependence.

Mavko *et al.* (1998) review a number of dispersion mechanisms, and emphasize the commonality between them. The behaviour is generally in three parts; a low-frequency regime without attenuation, a high-frequency regime again without attenuation and a transition zone in which dispersion and attenuation are significant. They suggest that in many cases the precise mechanism responsible for the dispersion is almost irrelevant and it is sufficient to understand this basic structure. We offer the results of this paper in that spirit. We seek to understand the effect of combining the standard Gassmann effect with fluid sensitive dispersion and hope that the resulting seismic signature will be at least partially independent of the underlying dispersion mechanism. We nevertheless will perform our calculations within the framework of the squirt flow theory of Chapman *et al.* (2002), largely in view of its computational simplicity and the ease with which it can be incorporated into reflectivity modelling algorithms.

In what follows we study numerically the effect of abnormally high dispersion and attenuation in the reservoir layer on reflection seismograms. We perform our calculations with a reflectivity algorithm which allows frequency dependent velocities and attenuations. We demonstrate that the frequency response is closely related to the AVO behaviour of the reflections. The model provides a consistent explanation for a number of frequency anomalies, which we have observed in seismic data.

ROCK PHYSICS MODELLING

Rock physics modelling methodologies which address the main challenges in carrying out AVO analysis, principally porosity–velocity transforms, velocity–density transforms, fluid substitution and shear-wave velocity prediction, are well established in the literature (Wyllie *et al.* 1956; Gardner *et al.* 1974; Castagna *et al.* 1985; Han *et al.* 1986; Gassmann 1951; Xu & White 1996). By contrast, many models that have been derived specifically to study frequency dependence in the elastic constants, (Hudson *et al.* 1996; Pointer *et al.* 2000; Tod 2001; Jakobsen & Hudson 2003; Jakobsen 2004; Jakobsen & Johansen 2005; van der Kolk *et al.* 2001; Hudson *et al.* 2001; Chapman *et al.* 2002; Chapman 2003) may not be well suited to address these practical problems. In addition, these models are typically formally restricted to low concentrations of inclusions, and may give unstable results when larger, and more realistic, concentrations are used.

In this paper we wish to provide a dispersion correction to an existing, usually empirical or semi-empirical, rock physics model, so that our ideas can be used in conjunction with the standard methodologies. Our method is based on that of Chapman *et al.* (2003). Specifically, our procedure is as follows. The input to our analysis will be a rock physics model: density and velocities as a function of porosity. Within the context of our more general modelling, these values are assumed to hold for propagation at some particular frequency ω_0, for saturation with a fluid of bulk modulus κ_f^0 and for assumed reference values of the technical parameters needed for the dispersive modelling—a timescale parameter τ_0 and crack density ε_0:

$$V_p = V_p(\phi \,|\, \omega = \omega_0, \kappa_f = \kappa_f^0, \varepsilon = \varepsilon_0, \tau = \tau_0); \tag{1}$$

$$V_s = V_s(\phi \,|\, \omega = \omega_0, \kappa_f = \kappa_f^0, \varepsilon = \varepsilon_0, \tau = \tau_0). \tag{2}$$

The innovation that we wish to make is to introduce an additional step at this point which allows us to account for fluid-sensitive attenuation and dispersion. We utilize the model of Chapman *et al.* (2002), which

takes the form:

$$C_{ijkl} = C_{ijkl}(\lambda, \mu, \omega, \tau, \phi, \varepsilon, \kappa_f). \quad (3)$$

Following the expressions given in the Appendix, we decompose this tensor into the form:

$$C_{ijkl} = C^{iso}_{ijkl}(\lambda, \mu) - C^{1}_{ijkl}(\lambda, \mu, \omega, \tau, \phi, \varepsilon, \kappa_f); \quad (4)$$

where the first term is the isotropic elastic tensor of the material without inclusions and the second term is the perturbation due to the presence of cracks and pores. Then, defining reference elastic constants as:

$$\bar{\lambda} = \rho V_p^2(\phi) - 2\rho V_s^2(\phi); \quad (5)$$

$$\bar{\mu} = \rho V_s^2(\phi); \quad (6)$$

we further define:

$$C^{iso}_{ijkl}(\Lambda, \mathrm{M}) = C^{iso}_{ijkl}(\bar{\lambda}, \bar{\mu}) + C^{1}\left(\bar{\lambda}, \bar{\mu}, \omega_0, \tau_0, \phi, \varepsilon_0, \kappa_f^0\right) \quad (7)$$

and then for arbitrary frequency, fluid bulk modulus and timescale parameter we define our elastic tensor as:

$$C_{ijkl} = C^{iso}_{ijkl}(\Lambda, \mathrm{M}) - C^{1}(\bar{\lambda}, \bar{\mu}, \omega, \tau, \phi, \varepsilon, \kappa_f). \quad (8)$$

In this way, our final elastic tensor reproduces the input rock physics model when the frequency and fluid saturation coincide with the assumptions of that model, but we are able to correct the model for changing frequency and fluid saturation.

NUMERICAL EXAMPLE

In this section we study numerically the effect of having a layer with strongly dispersive and attenuating properties within a standard reflectivity model. Specifically we will consider the case which simulates a shale encasing a sandstone layer, with only a weak contrast in elastic properties at the interface. We adapt our choice of material properties from the examples given in Castagna (1993). Since we wish to capture the concept of an attenuation anomaly in the reservoir, the shale will be assumed to have purely elastic (and isotropic) properties; the *P*-wave velocity will be 2743 m s^{-1}, *S*-wave velocity 1394 m s^{-1} and density 2060 kg m^{-3}. The properties of the sandstone are defined under water saturation and are taken as a *P*-wave velocity of 2790 m s^{-1} and *S*-wave velocity of 1463 m s^{-1} for propagation at 10 Hz. Porosity is assumed to be 30 per cent and the density is 2080 kg m^{-3} water saturated and 2060 kg m^{-3} gas saturated. We use a value of 400 MPa for the bulk modulus of the gas. The values used for the models considered in this paper are summarized in Table 1.

Fig. 2 illustrates the predicted dependence of *P*- and *S*-wave velocity and attenuation on frequency for water and gas saturation for these model parameters. We see the Gassmann effect in a reduction in the *P*-wave velocity when gas replaces water; this does not occur for the *S*-wave case because at low frequency the shear modulus is decoupled from the saturating fluid. The *P*-wave velocity shows greater variation with frequency than the *S*-wave velocity, with a substantial increase in the magnitude of dispersion occurring when gas is introduced. Likewise, *P*-wave attenuation is very high for gas saturation but this is not the case for *S* waves. It is quite possibly this effect, which permits the use of converted waves to image beneath gas clouds (Li *et al.* 2001) when the *P*-wave image is degraded by the presence of gas.

In the low- and high-frequency limits no attenuation occurs and we return to the familiar elastic case. Nevertheless, much insight can be gained by studying the behaviour of the reflection coefficient in these cases. Fig. 3 shows the predicted behaviour in the limits under both water and gas saturation. Note that these cases represent solutions to the simple problem of reflection of a plane wave from the interface between two elastic, isotropic media (Aki & Richards 1980). As is often the case in such examples, the introduction of gas changes the sign of the reflection, coefficient from positive to negative.

Since velocity in the dispersive layer is greater at high frequency than at low frequency, the normal incidence reflection coefficient under either water or gas saturation at high frequency is always greater than the corresponding coefficient at low frequency. Most importantly, we note that since the gas case has greater attenuation and dispersion than the water-saturated case, the high- and low-frequency limits are further apart for gas than they are for water saturation.

When we consider wave propagation, we will generally not be in either the high- or low-frequency regime. As the frequency changes, the reflection coefficient moves between the low- and high-frequency limits. What we expect from Fig. 3 is that when dispersion is important, reflections from the gas-saturated layer will experience a greater (in absolute value) reflection coefficient for their low-frequency components than they do for their high-frequency components. This will lead to an apparent redistribution of energy, which will shift the spectrum to lower frequencies. Conversely, the water-saturated case will see the spectrum biased towards the high frequencies.

This behaviour can be demonstrated with synthetic seismograms. We employ a reflectivity code (incorporated in the ANISEIS software package: Taylor 1990) which has a facility to specify a different complex elastic stiffness tensor for each frequency. The use of frequency-dependent complex velocities in reflectivity algorithms has been discussed in detail by Mallick & Frazer (1987). This procedure is appropriate for homogeneous media with frequency dependent properties, and neglects, for example, the possible generation of the slow *P* wave at the interface. For this calculation we assume an explosive source, ten receivers with a spacing of 55 m and a 35 Hz Ricker wavelet. For simplicity we will take a three layer model: a top layer of our shale with thickness 500 m, a 400 m thick sandstone with frequency dependent properties and then a half-space of the shale. This arrangement allows us to study the top reflection in isolation without the presence of tuning effects.

Fig. 4 shows the seismograms for the top PP reflection in four cases corresponding to different values of the timescale parameter τ, which controls the frequency regime, assuming gas saturation. Attempts have been made to estimate τ directly (Maultzsch *et al.* 2003), but in this study we confine ourselves to considering the influence of different τ values. The low- and high-frequency limits correspond to τ values of 10^{-6} and 100 s, respectively. We also show the results for τ values of 5×10^{-3}s and 5×10^{-2} s; in these cases dispersion effects are evident in the frequency band which we use for our calculations. As expected from Fig. 3, a decrease in amplitude is evident as we increase τ and, therefore, move from the low- to the high-frequency regime.

Less evidently there is a subtle frequency effect. We consider the average spectrum of the reflection that is the result of windowing the arrivals, performing a Fourier transform and stacking the resulting spectra in the frequency domain. The spectra for the five cases are

Table 1. Numerical values used in the computations. The sand velocities assume water saturation. In all cases, the reference frequency is 10 Hz, the reference value $\tau_0 = 2 \times 10^{-5}$, and $\varepsilon = \varepsilon_0 = 0.1$ throughout. The oil bulk modulus is assumed to be 800 MPa, and the gas bulk modulus is taken as 400 MPa.

Model 1	Vp (m s^{-1})	Vs (m s^{-1})	ρ-water sat. (g cc^{-1})	ρ-gas sat. (g cc^{-1})	ρ-oil sat. (g cc^{-1})	ϕ
Shale	2743	1394	2.06	–	–	–
Sand	2790	1463	2.08	2.06	–	30 per cent
Model 2						
Shale	3166	1689	2.32	–	–	–
Sand	2950	1800	2.3	–	2.28	15 per cent
Model 3						
Shale	2249	731	2.139	–	–	–
Sand	2771	1499	2.08	2.02	–	30 per cent

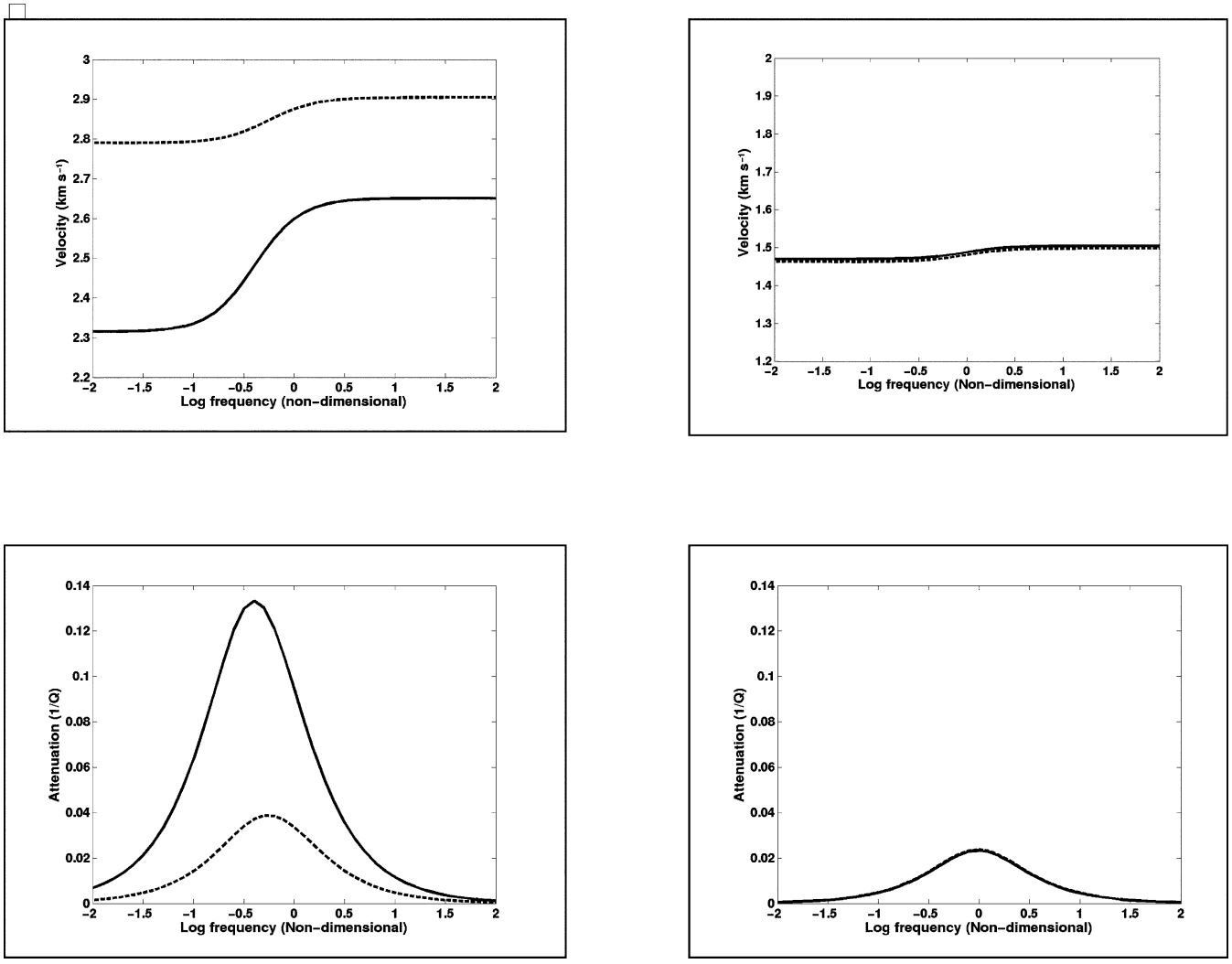

Figure 2. Predicted velocities and attenuations for Model 1 as a function of non-dimensional frequency $\omega\tau$. Top left—*P*-wave velocity, Top right, *S*-wave velocity, Bottom left—*P*-wave attenuation, Bottom right—*S*-wave attenuation. Dashed lines correspond to water saturation, solid lines to gas saturation.

shown in Fig. 5. The increase in amplitude is evident, along with a systematic frequency shift. The peak frequency is the same in both the high- and low-frequency limits, but as τ increases in the intermediate cases we see first a reduction in peak frequency and then an increase back to the value in the low τ case. Fig. 6 shows a particularly clear demonstration of this phenomenon. We form spectral ratios by dividing the spectrum for the water-saturated case (assumed to be in the low-frequency limit) by the spectra for gas

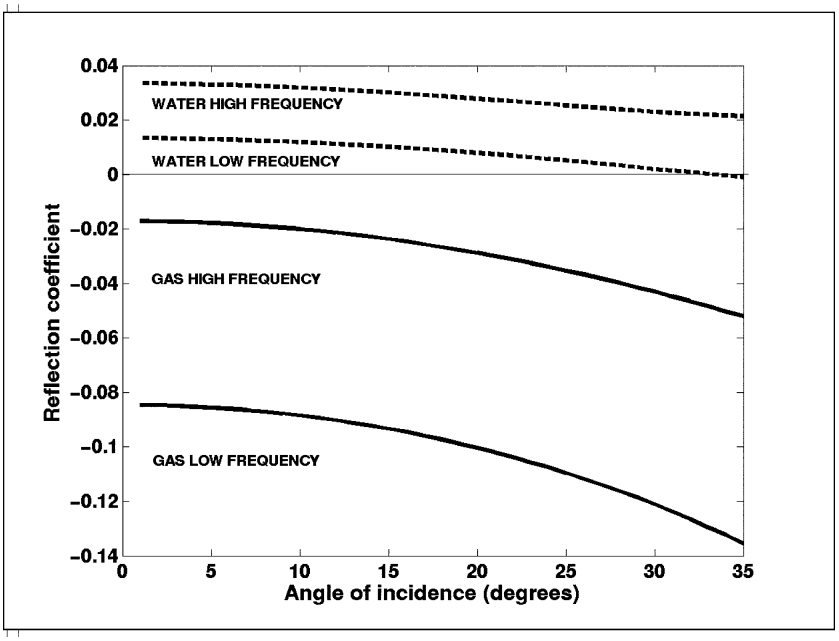

Figure 3. *P*-wave reflection coefficients in the low- and high-frequency limits for Model 1.

saturation in various frequency regimes. It is clear that this spectral ratio does not vary with frequency when we are in the limiting case, but there is a change with frequency for intermediate τ values.

These spectral variations occur for waves which have propagated from the source, through the elastic overburden, been reflected at the top of the frequency dependent layer and returned to the receiver. For reflections from the base of the attenuating layer there is an additional transmission effect of the attenuation, which in general depends on the thickness of the attenuating layer (Samec & Blangy 1992). Fig. 7 shows examples from the model where a sandstone layer of 150 m has been assumed and we display the low-frequency limit, the high-frequency limit and the attenuating case. The effect of attenuation is clear from the low amplitude of the base reflection in that case. The high-frequency energy travels with a higher velocity than the low-frequency energy, meaning that the wavelet is stretched between the traveltimes of the low- and high-frequency case. The resulting arrival is low frequency and has high frequencies concentrated at the head of the wavelet followed by a longer low-frequency tail.

DATA EXAMPLE—BRIGHT SPOT ANALYSIS

In general we do not always expect that replacing water saturation with hydrocarbon saturation will result in a change in the sign of the reflection coefficient. In the class III case of Rutherford and Williams (1989), the introduction of gas tends to lead to an increase in amplitude, as the reflection coefficient becomes more negative; this is the bright spot effect. Unfortunately, bright spots can be caused by factors other than hydrocarbon saturation, particularly local increases in porosity.

Fig. 8 shows an example of a bright spot on a stacked section—a significant increase in amplitude can be observed around CDP number 1300, for the reflection at 2.1 s. We wish to study this anomaly in more depth, and so define two zones; the first is a flank zone outside the anomaly in CDP's 1233–1243 and the second is within the anomaly, CDP's 1297–1307. The pre-stack time-migrated CDP gathers are summed within each zone to increase signal to noise ratio, and the results are shown in Fig. 9.

It is clear that the reflection of interest shows an increase in amplitude with offset in both zones, but that the effect is more pronounced within the anomaly. We now study the variation in frequency content between the two zones on the stacked section. Using a tapered 120 ms window we isolate the reflections in the two zones, perform a Fourier transform and stack the amplitude spectra in the Fourier domain, yielding an average spectrum for each zone. These spectra are shown in Fig. 10. We can clearly see the effect of tuning, and a change in the tuning frequency between the two zones, but it also appears that the anomaly is not only brighter but richer in low frequencies than the flank zone.

We now adapt our earlier numerical model for the case of a class III AVO anomaly. The shale is taken as having a *P*-wave velocity of 3166 m s^{-1}, an *S*-wave velocity of 1689 m s^{-1} and a density of 2320 kg m^{-3}. Under the same assumptions we modify the velocities of the sandstone to be 2950 m s^{-1} for *P* wave and 1800 m s^{-1} for the *S* wave, under water saturation at a frequency of 10 Hz. Porosity is assumed to be 15 per cent, and density 2300 kg m^{-3}. We also consider saturation with oil, whose bulk modulus is assumed to be 800 MPa, with density under oil saturation being assumed to be 2280 kg m^{-3}. The resulting predicted behaviour of the limiting values of the reflection coefficient is shown in Fig. 11. The general structure is similar to our earlier case, except that all the reflection coefficients in the region of interest are negative. Once again the low-frequency limits are lower in value than the corresponding high-frequency limits, although now the oil-saturated high-frequency reflection coefficient is higher than the low-frequency water-saturated reflection coefficient. This happens as a result of competition between the compressibility effect on velocity and the dispersion effect.

Synthetic seismograms corresponding to the earlier calculations were performed for various values of the timescale parameter τ, and for both water and oil saturation. A 400-m-thick sandstone layer was

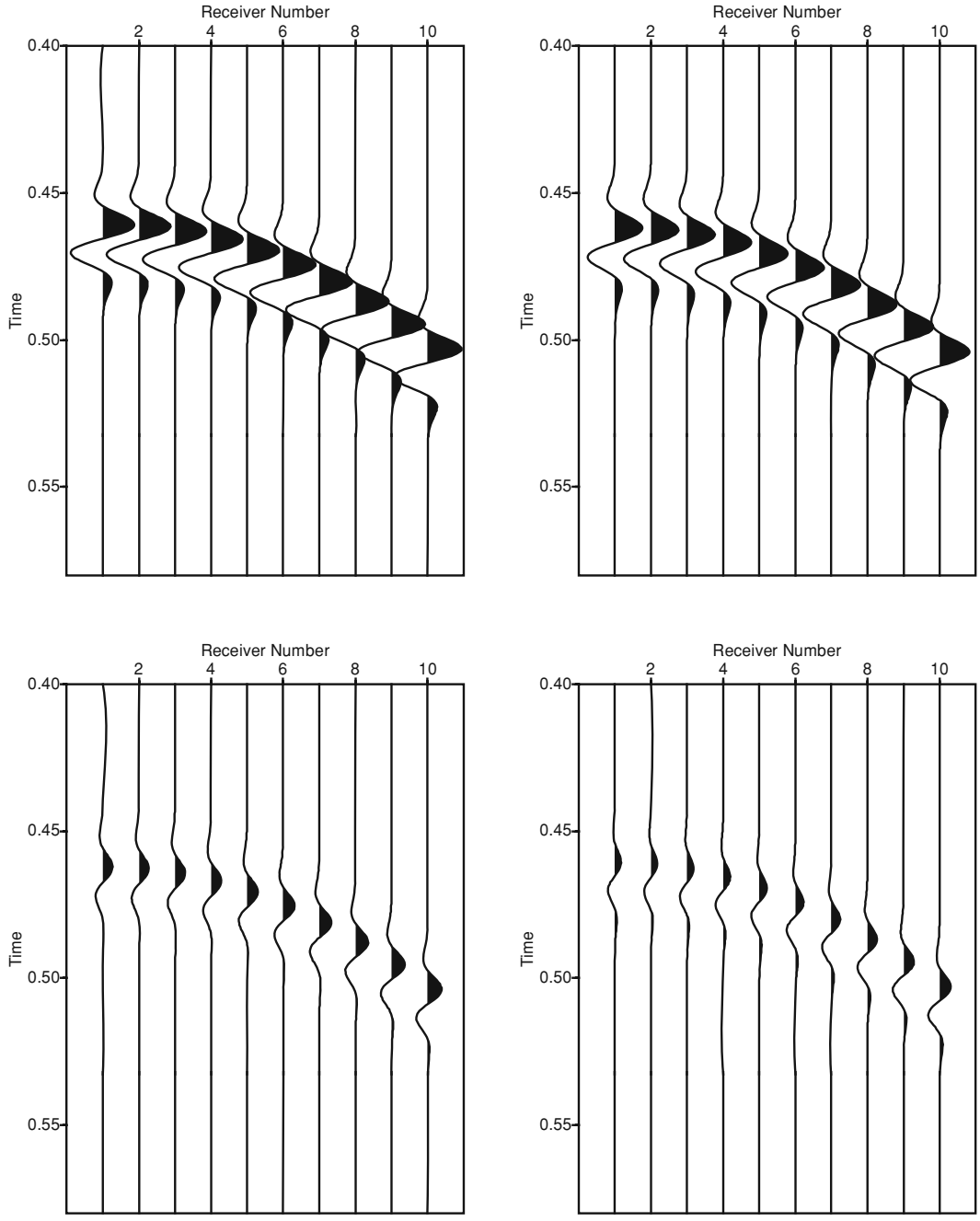

Figure 4. Synthetic seismograms for Model 1 assuming τ values of: Top left—10^{-6} s, Top right—5×10^{-3} s, Bottom left—5×10^{-2} s and Bottom right—100 s.

used so as to avoid interference between the top and base reflections. The top reflections were windowed, Fourier transformed and their spectra stacked in the frequency domain. We then formed spectral ratios by dividing, for each frequency, the spectrum calculated for water saturation by that for gas saturation, where for the gas case a range of τ values were used. In Fig. 12 we compare the spectral ratio for the low-frequency (Gassmann) limit, the dispersive case when $\tau = 2 \times 10^{-2}$ s and the result of performing the same operation on the data displayed in Fig. 10.

We now study the effect of tuning on this analysis. When we make the thickness of the sandstone layer 70 m, the reflections from the top and base of the layer interfere giving us notches in the spectrum. The situation is further complicated by the transmission effect of attenuation as the base reflection travels through the attenuating layer. Nevertheless, dispersion still has an influence on the reflected spectra. Fig. 13 shows the reflected average spectra in the low-frequency limit for water and oil saturation, together with the attenuating gas-saturated case. A relative boost to the low frequencies in the attenuating case can still be seen.

DATA EXAMPLE—DIM SPOT ANALYSIS

In the class I case of Rutherford and Williams (1989), characterized by a low impedance shale overlying a higher impedance sand, the

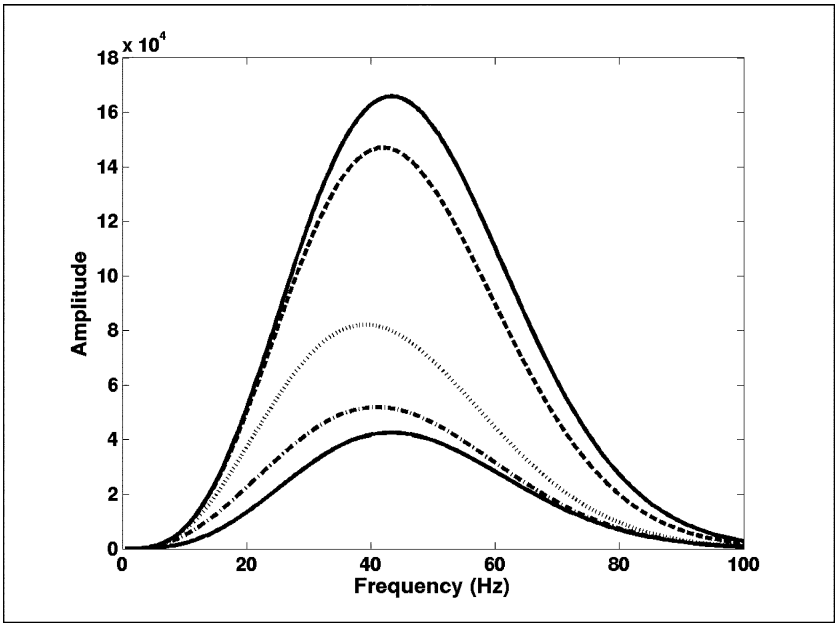

Figure 5. Average spectra of the top reflections for Model 1, assuming τ values of (from the bottom) 100s, 5×10^{-2} s, 2×10^{-2} s, 5×10^{-3} s and 10^{-6} s.

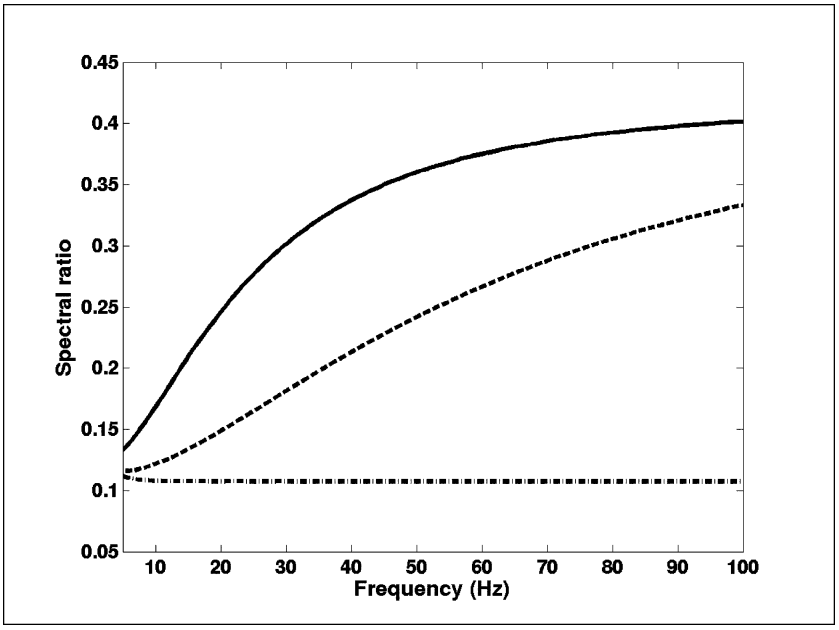

Figure 6. Spectral ratios formed by dividing the average spectrum of the water-saturated case (low-frequency limit), by the gas-saturated average spectra with τ values of 10^{-6} s (dashed-dotted line), 2×10^{-2} s (dashed line) and 5×10^{-2} s (solid line).

introduction of gas often leads to a dimming of amplitude. Fig. 14 shows an example of a dim spot, a local decrease in amplitude, around CDP's 1660–1680 for the reflection just above 3.4 s.

Once again we define two zones along the same reflection, one inside the anomaly and one outside, to compare the behaviour. The zone outside the anomaly is taken to be CDP numbers 1629–1635, while the anomaly is taken to be at CDP numbers 1665–1671. Summing the pre-stack CDP gathers in each case we arrive at Fig. 15. A very different character to the previous example is evident. The amplitudes decrease with offset; this is indicative of the Class I case.

To study the comparative frequency response of the two cases on the stack we once again window the reflection in the two zones with a 120 ms tapered window, Fourier transform and stack the amplitude spectra in the frequency domain. The result is given in Fig. 16. It is evident that the anomaly has lower amplitude than that outside the anomaly, but it also appears to have higher frequency. Again tuning phenomena are suggested, with an apparent notch around 40 Hz.

We now adapt our modelling framework to study theoretically a dim spot, changing the shale velocity to 2249 m s^{-1} for the *P* wave and 731 m s^{-1} for the *S* wave, the density being assumed to

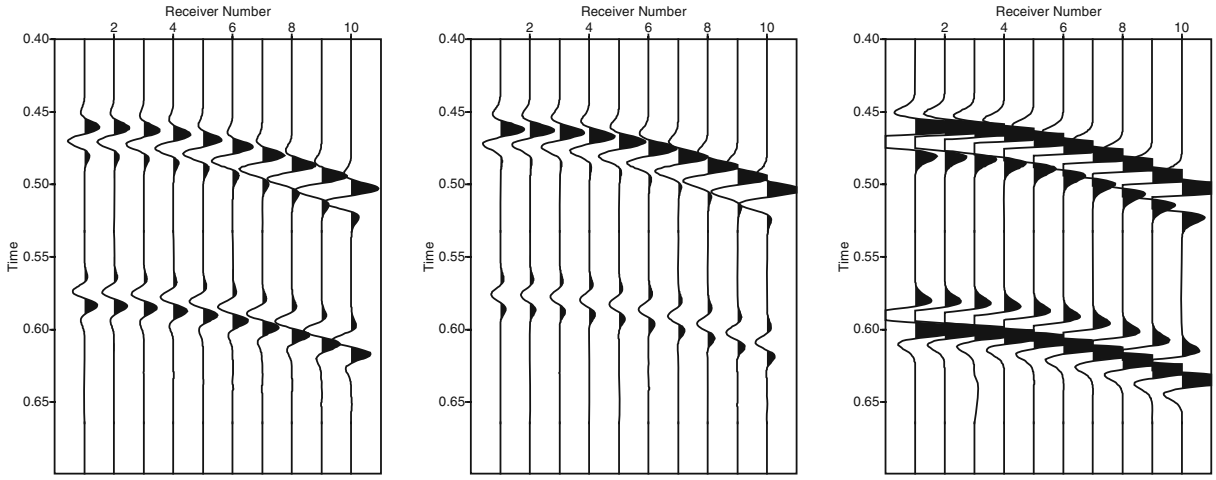

Figure 7. Synthetic seismograms for Model 1 with a 150 m thick gas reservoir layer illustrating the top and base reservoir reflections for τ values of 100 s (left), 5×10^{-2} s (centre) and 10^{-6} s (right). The influence of attenuation as a transmission mechanism is evident in the centre diagram.

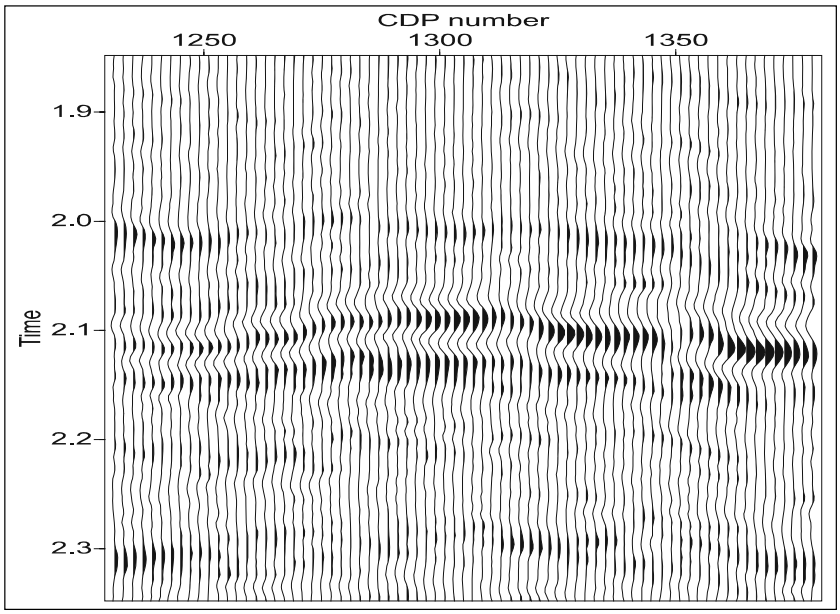

Figure 8. Stacked seismic section showing an anomaly (bright spot) centred around CDP 1300 at 2.1 s.

be 2139 kg m^{-3}. The sand velocities are 2771 m s^{-1} for *P* wave and 1499 m s^{-1} for *S* wave under water saturation at a frequency of 10 Hz. Porosity is 30 per cent and density 2080 kg m^{-3}. We consider saturating fluids of water and gas with bulk modulus 400 MPa, with the gas-saturated density being 2020 kg m^{-3}. The predicted behaviour of the limiting values of the reflection coefficient is shown in Fig. 17. This follows the same general structure as before, except that it is clear that the gas-saturated case is indeed predicted to have a lower amplitude than the water-saturated case. It should be noted that it is the low frequencies, which are predicted to have the lowest amplitude in the gas-saturated case; indeed a phase reversal is predicted in the low-frequency limit.

We now repeat the analysis that we performed for the bright spot in the previous case. We calculate the spectral ratio between the flank zone spectrum and the anomaly spectrum. Spectral ratios are also formed between the low-frequency (Gassmann) water-saturated case and both the Gassmann gas-saturated case and the attenuating gas-saturated case assuming $\tau = 5 \times 10^{-2}$ s. These three cases are compared in Fig. 18. The Gassmann case does not give a ratio constant with frequency in this case because of the frequency and offset dependent zero crossing of the reflection coefficient implied by the phase change present in the low-frequency gas-saturated curve. In contrast to the preceding example, the other two spectral ratios have negative slope, and that for the model with dispersion is comparable to the data curve.

The trend is still visible when we introduce tuning by making the thickness of the sandstone layer 70 m. Fig. 19 shows the spectra in the low-frequency limit together with the gas-saturated spectrum in the attenuating case. The high frequencies have clearly been boosted by the effect of dispersion.

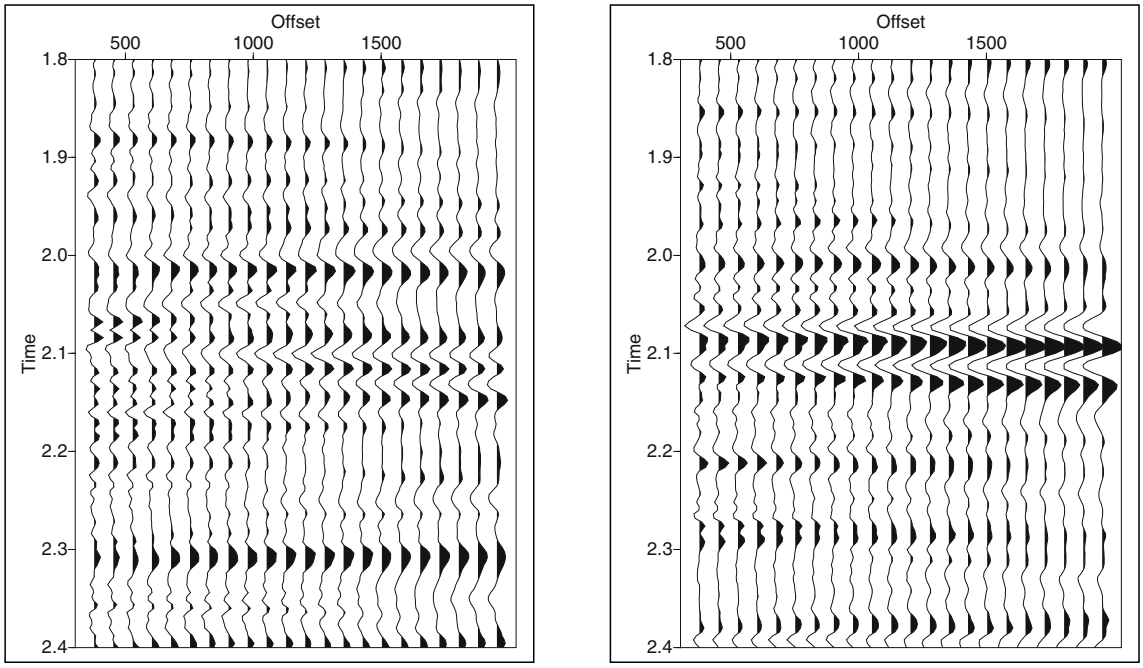

Figure 9. Pre-stack CDP supergathers corresponding to the zone outwith the anomaly (left) and within the anomaly (right).

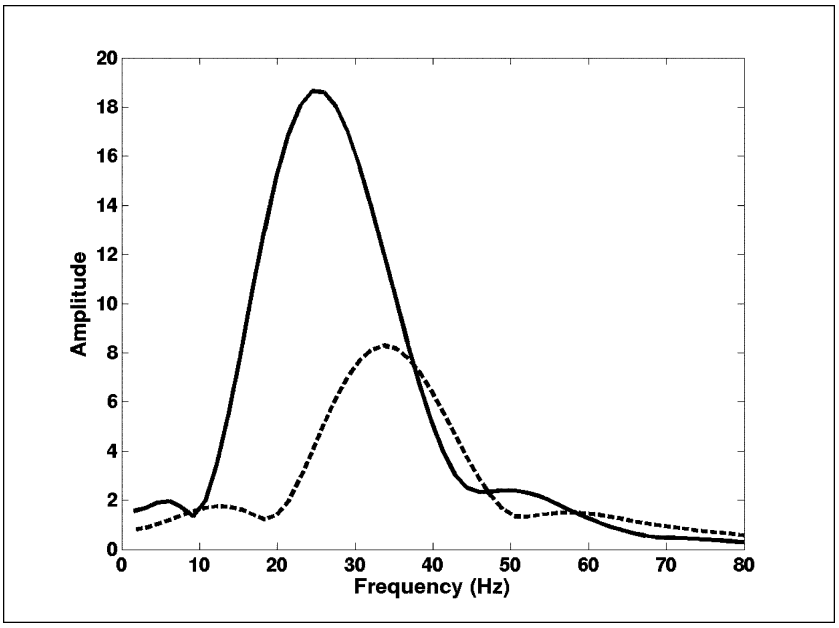

Figure 10. Average spectra from the stacked section outwith the bright spot anomaly (dashed line) and within the bright spot anomaly (solid line).

DISCUSSION AND CONCLUSIONS

This paper proceeds from the hypothesis that hydrocarbon saturation is associated with abnormally high values of dispersion and attenuation. Such an effect can be expected from laboratory measurements, but many direct measurements from borehole data demonstrate similar behaviour.

We have identified two possible mechanisms for the increase of attenuation, but we believe that the identification of zones of high attenuation can aid exploration even if we do not know the precise mechanism that is responsible. Our interest lies in determining the seismic signature of combining the standard Gassmann effect with fluid sensitive dispersion, and our choice of modelling is perhaps the simplest way to combine these effects.

Many techniques have been developed in the framework of both viscoelastic and poroelastic theory to treat the problem of reflection and transmission at an interface (see Carcione 2001, for a comprehensive review). Our results are based on a rather simple equivalent medium theory, which holds that the fluid-saturated rock may be replaced by a homogeneous isotropic equivalent material whose velocities and attenuations depend on frequency. The theory provides an explanation as to why hydrocarbon saturation should give rise to

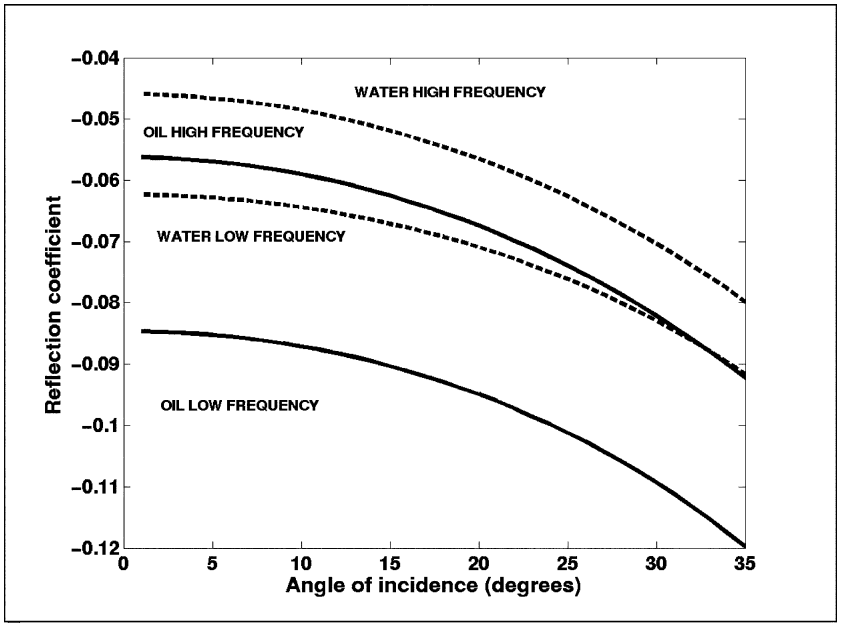

Figure 11. *P*-wave reflection coefficients in the low- and high-frequency limits for Model 2, illustrating our conceptual model of an oil induced bright spot on a class III interface.

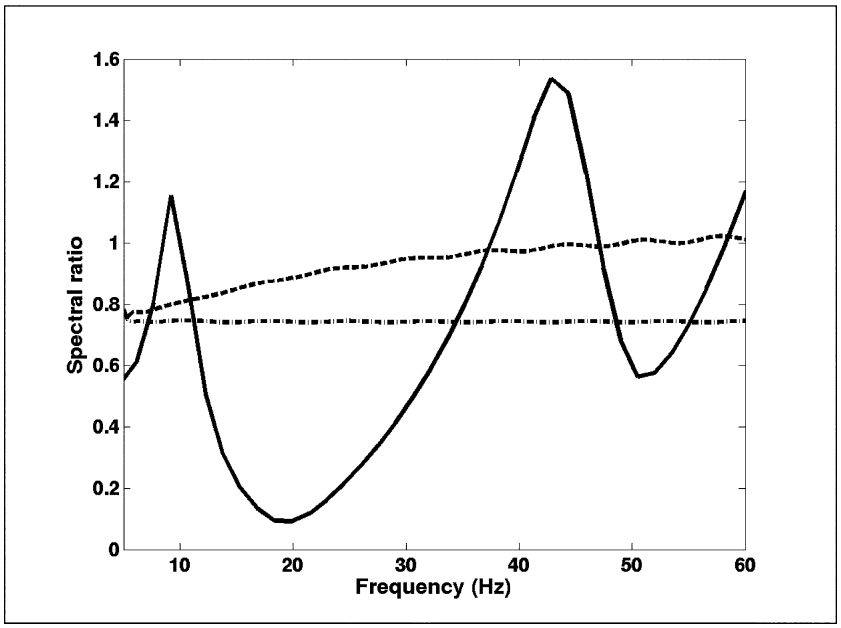

Figure 12. Spectral ratios formed by dividing the water-saturated average spectrum (low-frequency limit) for synthetic data by the oil-saturated average spectrum assuming τ values of 10^{-6} s (dashed-dotted line) and 5×10^{-2} s (dashed line). These are compared to the spectral ratio of the average spectrum outside the anomaly to that within it from the stacked data (solid line).

attenuation anomalies, but also predicts that this attenuation should be associated with significant velocity dispersion. This velocity dispersion gives rise to frequency dependence of impedance, and hence when we match displacement and traction at the interface we find a frequency dependent reflection coefficient. For Q values typical of those observed in hydrocarbon reservoirs we find that this effect is very significant for interpretation of the AVO response. Poroelastic developments have treated the fluid dynamics at the interface very thoroughly, but in these studies the magnitude of the velocity dispersion associated with the hydrocarbon deposit has been much smaller. To capture the concept of an attenuation anomaly in the reservoir we assume a purely elastic overburden. It should be borne in mind that this is an unrealistic oversimplification. Nevertheless it serves to focus attention on the fact that the existence of dispersion leads to a frequency dependent reflection coefficient as well as attenuation during transmission. The central point of our paper is to show that fluid-related dispersion is a strong candidate mechanism for the commonly observed frequency anomalies in seismic data.

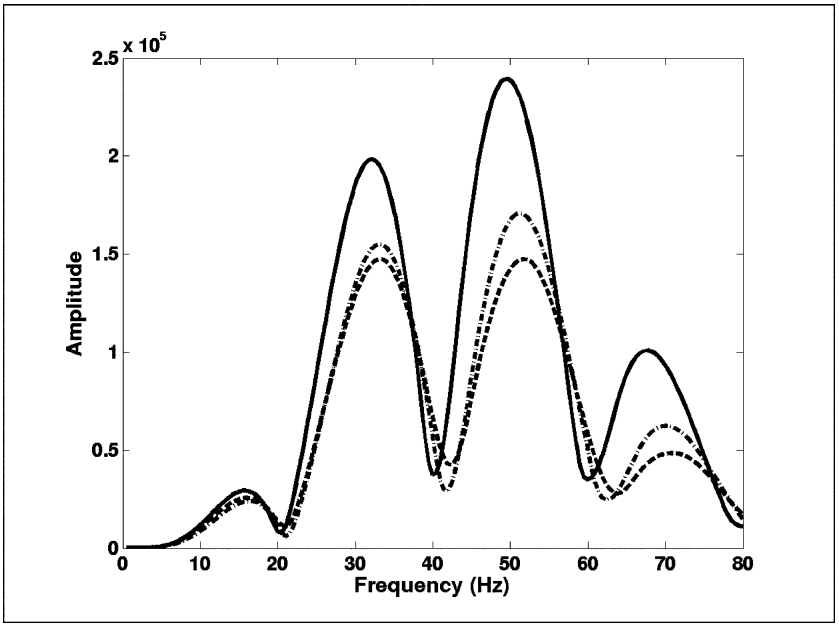

Figure 13. Average spectra for Model 2 with the reservoir being taken to be 70 m thick and assuming a τ value of 10^{-6} s for water saturation (dashed line) and oil saturation (solid line). The dotted-dashed line is for oil saturation assuming a τ value of 5×10^{-2} s.

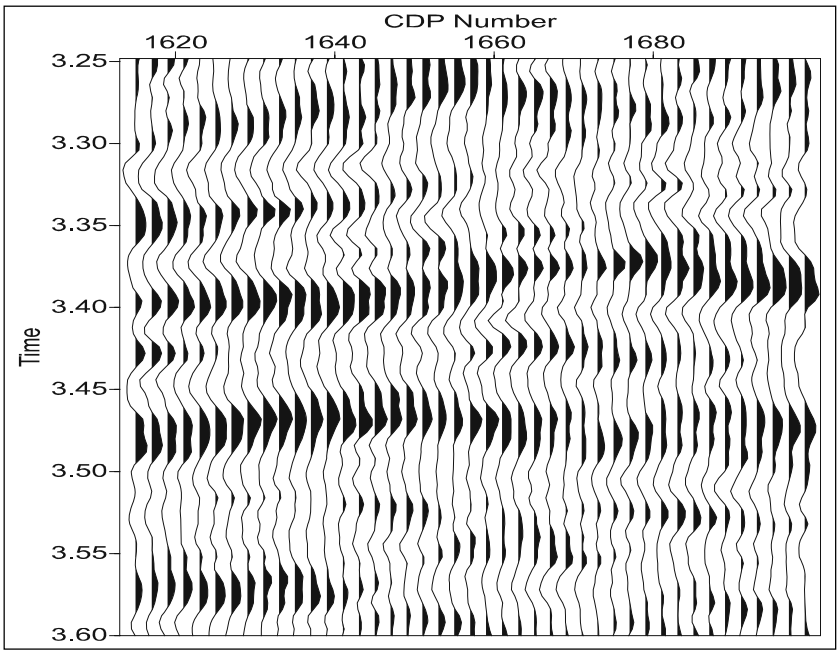

Figure 14. Stacked seismic section showing an anomaly (dim spot) centred around CDP 1670 above 3.4 s.

This point does not follow if we model attenuation by the traditional means of assigning a frequency independent imaginary part to the elastic tensor (MacBeth 1999).

We arrive at an extended version of the Rutherford & Williams (1989) framework in which the frequency response is coupled to the AVO behaviour at the interface. The seismic data, which we show fit plausibly into this framework. The model also explains the widely noted tendency for bright spots to be rich in low frequencies (Taner *et al.* 1979). While the theory is rather straightforward, some of the predictions are counterintuitive; particularly the prediction in our dim-spot example that, through the frequency dependent reflection coefficient, the existence of abnormally high attenuation can actually boost the high frequencies of the reflections rather than attenuating them as might be naively supposed. If this effect is important, it will add an extra layer of complexity to the uncertainties in Q estimation (White 1992).

We wish to make clear that we stop short of advocating a petrophysical interpretation of the data anomalies which we present. We lack the well control and reservoir engineering information which could support such an interpretation. Thus, we regard the data as illustrative but equivocal. Furthermore, we have not addressed the suggestion that seismic processing induces systematic frequency

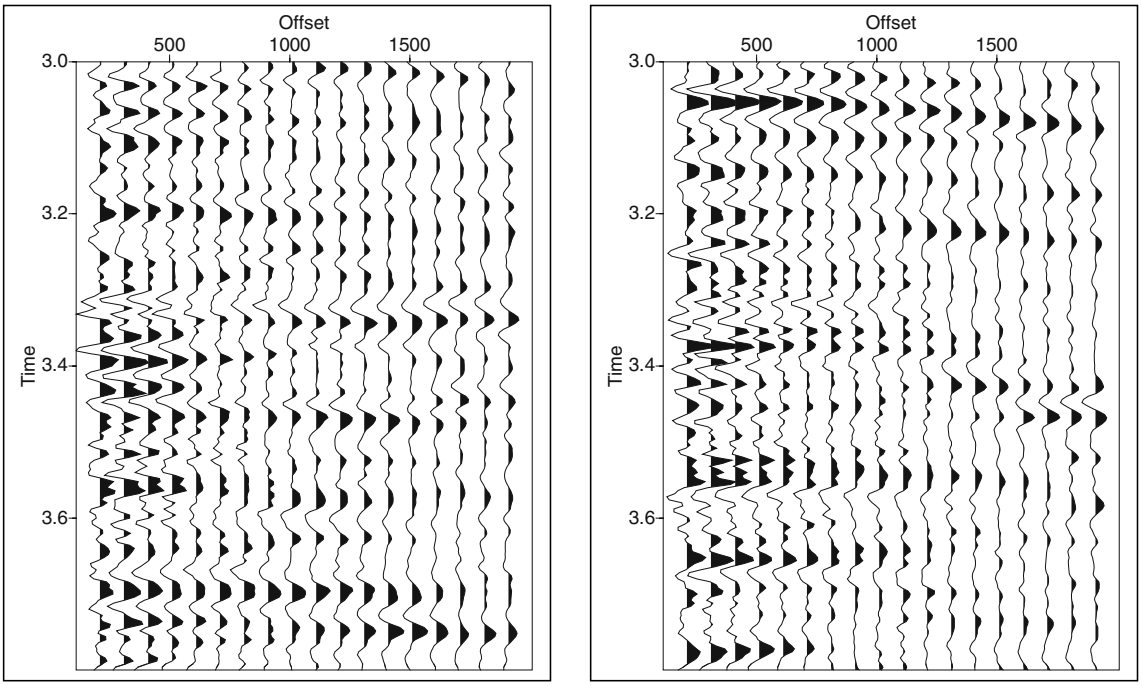

Figure 15. Pre-stack CDP supergathers corresponding to the zone outwith the anomaly (left) and within the anomaly (right).

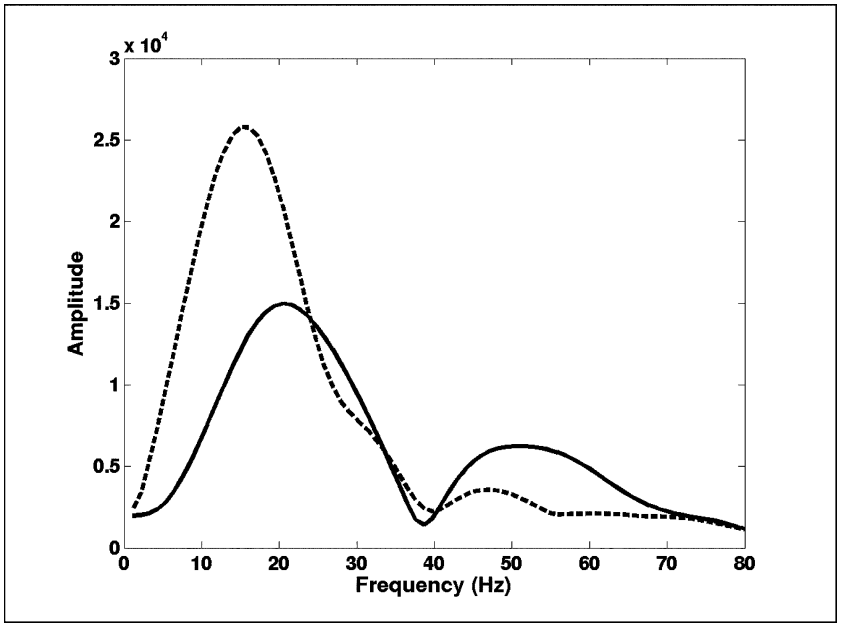

Figure 16. Average spectra from the stacked section outwith the dim-spot anomaly (dashed line) and within the dim-spot anomaly (solid line).

anomalies associated with hydrocarbon deposits (Ebrom 2004) nor attempted to remove any structural influence (Wang *et al.* 2002). Nevertheless, the application of the ideas we present to other data sets, particularly 3-D seismic, time lapse and VSP data is expected to shed considerable light on the problem, particularly if we extend the analysis to consider anisotropy (Lynn 2004). We expect that the application of spectral decomposition methods to such data will reveal whether the spectral response to hydrocarbon saturation is well captured by a combination of the Gassmann effect and tuning or whether the trends suggested by this study can be used to improve the characterization of hydrocarbon reservoirs.

ACKNOWLEDGMENTS

This work is presented with the permission of the Executive Director of the British Geological Survey (NERC) and is supported by the sponsors of the Edinburgh Anisotropy Project: BG, BGP,

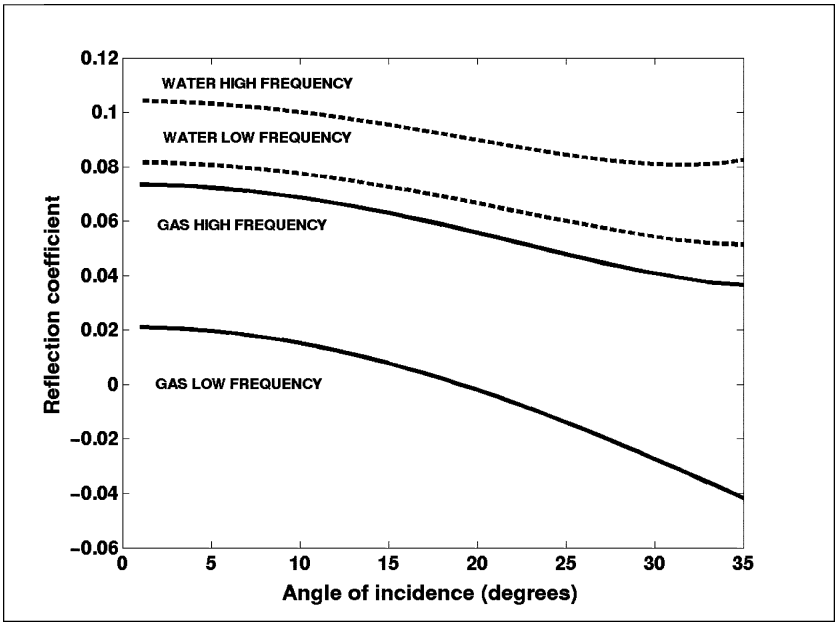

Figure 17. *P*-wave reflection coefficients in the low- and high-frequency limits for Model 3 under water and gas saturation, illustrating our conceptual model of a gas induced dim spot on a class I interface.

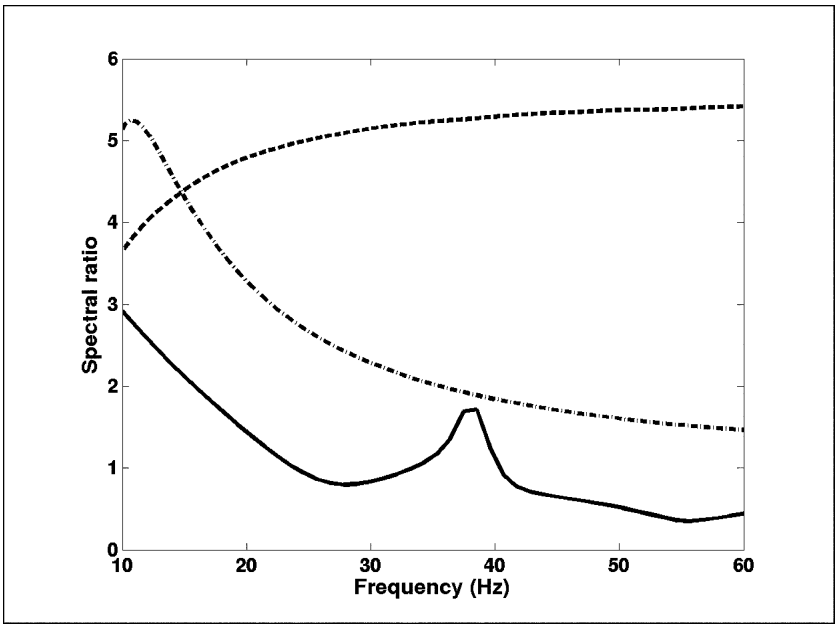

Figure 18. Spectral ratios formed by dividing the water-saturated average spectrum (low-frequency limit) for Model 3 synthetic data by the gas-saturated average spectrum assuming τ values of 10^{-6} s (dashed line) and 5×10^{-2} s (dashed-dotted line). These are compared to the spectral ratio of the average spectrum outside the anomaly to that within it from the stacked data (solid line).

BP, Chevron, CNPC, ConocoPhillips, ENI-Agip, ExxonMobil, GX Technology, Hydro, Kerr-McGee, Landmark, Marathon, PDVSA, Schlumberger, Shell, Total and Veritas DGC. We are grateful to Sonja Maultzsch (Total) for many discussions on this topic. Our particular gratitude goes to David Taylor of Macroc Ltd, for his help with the computation of synthetic seismograms in the ANISEIS software package. We thank Jose Carcione and an anonymous reviewer for constructive reviews which improved the manuscript.

REFERENCES

Aki, K. & Richards, P.G., 1980. *Quantitative Seismology: Theory and Methods*, W.H. Freeman and Co., San Francisco.

Assefa, S., McCann, C. & Sothcott, J., 1999. Attenuation of *P*- and *S*-waves in limestones, *Geophys. Prospect.,* **47,** 359–392.

Backus, G.E., 1962. Long-wave elastic anisotropy produced by horizontal layering, *J. geophys. Res.,* **67,** 4427–4440.

Batzle, M., Hofmann, R., Han, D.-H. & Castagna, J.P., 2001. Fluids and

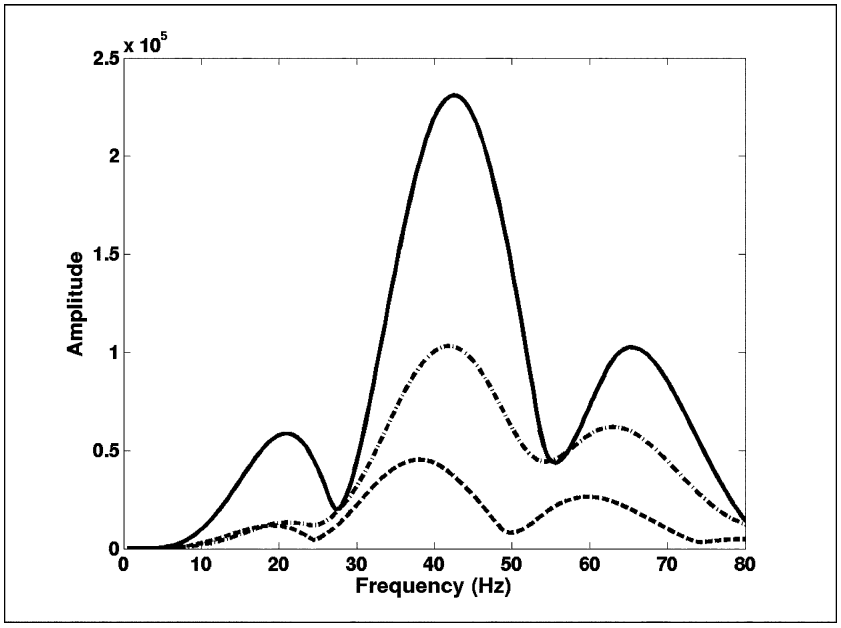

Figure 19. Average spectra for the Model 3 synthetic data with the reservoir being taken to be 70 m thick and assuming a τ value of 10^{-6} s for water saturation (solid line) and gas saturation (dashed line). The dotted-dashed line is for gas saturation assuming a τ value of 5×10^{-2} s.

frequency dependent seismic velocity of rocks, *The Leading Edge,* **2,** 168–171.

Batzle, M. & Wang, Z., 1992. Seismic properties of pore fluids, *Geophysics,* **57,** 1396–1408.

Best, A.I., McCann, C. & Sothcott, J., 1994. The relationships between the velocities, attenuations and petrophysical properties of reservoir sedimentary rocks, *Geophys. Prospect.,* **42,** 151–178.

Biot, M.A., 1956. Theory of propagation of elastic waves in a fluid saturated porous solid. I. Low frequency range and II. Higher-frequency range, *J. acoust. Soc. Am.,* **28,** 168–191.

Bourbie, T., Coussy, O. & Zinszner, B., 1987. *Acoustics of Porous Media*, Gulf Publishing Co., Houston.

Burnett, M.D., Castagna, J.P., Mendez-Hernandez, E., Rodriguez, E.Z., Garcia, L.F, Martinez-Vasquez, J.T., Telles-Aviles, M. & Vila-Villasenor, R., 2003. Application of spectral decomposition to gas basins in Mexico, *The Leading Edge,* **22,** 1130–1134.

Carcione, J.M., 1998. Viscoelastic effective rheologies for modelling wave propagation in porous media, *Geophys. Prospect.,* **46,** 249–270.

Carcione, J.M., 1999. Effects of vector attenuation on AVO of offshore reflections, *Geophysics,* **64,** 815–819.

Carcione, J.M., 2001. *Wave Fields in Real Media*, Theory and numerical simulation of wave propagation in anisotropic, anelastic and porous media, Pergamon Press.

Carcione, J.M., Helle, H.B. & Zhao, T., 1998. Effects of attenuation and anisotropy on reflection amplitude versus offset, *Geophysics,* **63**(5), 1652–1658.

Carcione, J.M., Helle, H.B. & Pham, N., 2003. White's model for wave propagation in partially saturated rocks: Comparision with poroelastic numerical experiments, *Geophysics,* **68,** 1389–1398.

Castagna, J.P., 1993. AVO analysis—tutorial and review, in *Offset-Dependent Reflectivity—Theory and Practice of AVO analysis*,Vol. 8, pp. 3–36, eds Castagna, J.P. & Backus, M.M., Investigations in Geophysics, Soc. Expl. Geophys., Tulsa, Oklahoma.

Castagna, J.P., Batzle, M.L. & Eastwood, R.L., 1985. Relationships between compressional-wave and shear-wave velocities in clastic silicate rocks, *Geophysics,* **50,** 551–570.

Castagna, J.P., Batzle, M.L. & Kan, T.K., 1993. Rock Physics—The link between rock properties and AVO response, in *Offset-Dependent Reflectivity—Theory and Practice of AVO analysis*,Vol. 8, pp. 135–171, eds Castagna, J.P. & Backus, M.M., Investigations in Geophysics, Soc. Expl. Geophys., Tulsa, Oklahoma.

Castagna, J.P., Sun, S. & Seigfried, R.W., 2003. Instantaneous spectral analysis: detection of low-frequency shadows associated with hydrocarbons, *The Leading Edge,* **22,** 120–127.

Chapman, M., 2003. Frequency dependent anisotropy due to meso-scale fractures in the presence of equant porosity, *Geophys. Prospect.,* **51,** 369–379.

Chapman, M., Zatsepin, S.V. & Crampin, S., 2002. Derivation of a microstructural poroelastic model, *Geophys. J. Int.,* **151,** 427–451.

Chapman, M., Maultzsch, S., Liu, E. & Li, X.-Y., 2003. The effect of fluid saturation in a multi-scale equant porosity model, *J. appl. Geophys.,* **54,** 191–202.

Dasgupta, R. & Clark, R.A., 1998. Estimation of Q from surface seismic reflection data, *Geophysics,* **63,** 2120–2128.

Dasios, A., Astin, T. & McCann, C., 2001. Compressional-wave Q estimation from full-waveform sonic data, *Geophys. Prospect.,* **49,** 353–373.

Denneman, A.I.M., Drijkoningen, G.G., Smeulders, D.M.J. & Wapenaar, K., 2002. Reflection and transmission of waves at a fluid/porous-medium interface, *Geophysics,* **67,** 282–291.

Deresiewicz, H. & Rice, J.T., 1964. The effect of boundaries on wave propagation in a liquid-filled porous solid, V—transmission across a plane interface, *Bull. seism. Soc. Am.,* **54,** 409–416.

Dutta, N.C. & Ode, H., 1979. Attenuation and dispersion of compressional waves in fluid-filled porous rocks with partial gas saturation (White model), Part I: Biot theory, Part II: results, *Geophysics,* **44,** 1777–1805.

Dutta, N.C. & Ode, H., 1983. Seismic reflections from a gas-water contact, *Geophysics,* **48,** 148–162.

Dvorkin, J., Mavko, G. & Nur, A., 1995. Squirt flow in fully saturted rocks, *Geophysics,* **62,** 106–117.

Dvorkin, J. & Uden, R., 2004. Interpreter's corner—seismic wave attenuation in a methane hydrate reservoir, *The Leading Edge,* **23**(8), 730–732.

Ebrom, D., 2004. The low frequency gas shadow on seismic sections, *The Leading Edge,* **23**(8), 772.

Endres, A.L. & Knight, R.J., 1997. Incorporating pore geometry and fluid pressure communication into modelling the elastic behaviour of porous rocks, *Geophysics,* **62,** 106–117.

Eshelby, J.D., 1957. The determination of the elastic field of an ellipsoidal inclusion, and related problems, *Proc. R. Soc. Lond., A.,* **241,** 376–396.

Gardner, G.H.F., Gardner, L.W. & Gregory, A.R., 1974. Formation velocity and density—the diagnostic basis for stratigraphic traps, *Geophysics,* **39,** 770–780.

Gassmann, F., 1951. Uber die elastizitat poroser medien: *Vier. der Natur. Gesellschaft in Zurich,* **96,** 1–23.

Geertsma, J. & Smit, D.C., 1961. Some aspects of elastic wave propagation in fluid-saturated porous solids, *Geophysics,* **26,** 169–181.

Goloshubin, G.M. & Bakulin, A.V., 1998. Seismic reflectivity of a thin porous fluid-saturated layer versus frequency, *68th Ann. Int. Mtg. Soc. Expl. Geophys.,* 976–979.

Gurevich, B., 1996. Discussion on: Wave propagation in heterogeneous, porous media: A velocity-stress, finite difference method, by N. Dai, A. Vafidis and E.R. Kanasewich (March-April 1995 Geophysics, pp. 327–340), *Geophysics,* **61,** 1230–1232.

Gurevich, B., Ciz, R. & Denneman, A.I.M., 2004. Simple expressions for normal incidence reflection coefficients from an interface between fluid-saturated porous materials, *Geophysics,* **69,** 1372–1377.

Gurevich, B., Zyrianov, V.B. & Lopatnikov, S.L., 1997. Seismic attenuation in finely layered porous rocks: Effects of fluid flow and scattering, *Geophysics,* **62,** 319–324.

Gurevich, B. & Schoenberg, M., 1999. Interface conditions for Biot's equations of poroelasticity, *J. acoust. Soc. Am.,* **105,** 2585–2589.

Han, D.H., Nur, A. & Morgan, D., 1986. Effects of porosity and clay content on wave velocities in sandstones, *Geophysics,* **51,** 2093–2107.

Harris, P.E., Kerner, C. & White, R.E., 1997. Multichannel estimation of frequency-dependent Q from VSP data, *Geophys. Prospect.,* **45,** 87–109.

Holzner, R., Eschle, P., Zurcher, H., Lambert, M., Graf, R., Dangel, S. & Meier, P.F., 2005. Applying microtremor analysis to identify hydrocarbon reservoirs, *First Break,* **23,** 41–48.

Hudson, J.A., Liu, E. & Crampin, S., 1996. The mechanical properties of materials with interconnected cracks and pores, *Geophys. J. Int.,* **124,** 105–112.

Hudson, J.A., Pointer, T. & Liu, E., 2001. Effective medium theories for fluid saturated materials with aligned cracks, *Geophys. Prospect.,* **49,** 509–522.

Jakobsen, M., 2004. The interacting inclusion model of wave induced fluid flow, *Geophys. J. Int.,* **158,** 1168–1176.

Jakobsen, M. & Hudson, J.A., 2003. Viscoelastic waves in rock like composites, *Stud geophys. Geod.,* **47,** 793–826.

Jakobsen, M. & Johansen, T.A., 2005. The effects of drained and undrained loading in visco-elastic waves in rock-like composites, *Int. J. Solids and Structures,* **42,** 1597–1611.

Kelder, O. & Smeulders, D.M.J., 1997. Observation of the Biot slow wave in water-saturated Nievelsteiner sandstone, *Geophysics,* **62,** 1794–1796.

King, M.S. & Marsden, J.R., 2002. Velocity dispersion between ultrasonic and seismic frequencies in brine-saturated reservoir sandstones, *Geophysics,* **67,** 254–258.

Klimentos, T., 1995. Attenuation of *P*- and *S*-waves as a method of distinguishing gas and condensate from oil and water, *Geophysics,* **60,** 447–458.

Klimentos, T. & McCann, C., 1988. Why is the Biot slow wave not observed in real rocks?, *Geophysics,* **53,** 1605–1609.

Korneev, V.A., Goloshubin, G.M., Daley, T.M. & Silin, D.B., 2004. Seismic low-frequency effects in monitoring fluid-saturated reservoirs, *Geophysics,* **69,** 522–532.

Le Ravalec, M. & Gueguen, Y., 1996. High- and low-frequency elastic moduli for a saturated porous/cracked rock—differential self consistent and poroelastic theories, *Geophysics,* **61,** 1080–1091.

Li, X.-Y., Dai, H., Mueller, M.C. & Barkved, O.I., 2001. Compensating for the effect of gas clouds on C-wave imaging: A case study from Valhall, *The Leading Edge,* **20,** 111–117.

Liu, Y., 2004. Seismic 'low frequency shadows' for gas sand reflection, *74th Ann. Int. Mtg: Soc. of Expl. Geophys.,* 1563–1566.

Luh, P.C., 1993. Wavelet attenuation and AVO, in *Offset-Dependent Reflectivity—Theory and Practice of AVO analysis*, Vol. 8, pp. 190–198, eds Castagna, J.P. & Backus, M.M., Investigations in Geophysics, Soc. Expl. Geophys., Tulsa, Oklahoma.

Lynn, H.B., 2004. The winds of change: Anisotropic rocks—their preferred direction of fluid flow and their associated seismic signatures, Part I, *The Leading Edge,* **11,** 1156–1162.

MacBeth, C., 1999. Azimuthal variation in *P*-wave signatures due to fluid flow, *Geophysics,* **64,** 1181–1192.

Mallick, S. & Frazer, L.N., 1987. Practical aspects of reflectivity modelling, *Geophysics,* **52,** 1355–1364.

Marion, D.P., Mukerji, T. & Mavko, G., 1994. Scale effects on velocity dispersion: From ray to effective medium theories in stratified media, *Geophysics,* **59,** 1613–1619.

Maultzsch, S., Chapman, M., Liu, E. & Li, X-Y., 2003. Modeling frequency-dependent seismic anisotropy in fluid-saturated rock with aligned fractures: implication of fracture size estimation from anisotropic measurements, *Geophys. Prospect.,* **51,** 381–392.

Mavko, G. & Jizba, D., 1991. Estimating grain-scale fluid effects on velocity dispersion in rocks, *Geophysics,* **56,** 1940–1949.

Mavko, G. & Nur, A., 1975. Melt squirt in the asthenosphere, *J. geophys. Res.,* **80,** 1444–1448.

Mavko, G., Mukerji, T. & Dvorkin, J., 1998. *The Rock Physics Handbook*, Cambridge University Press.

Mazzotti, A., 1991. Amplitude, phase and frequency versus offset applications, *Geophys. Prospect.,* **39,** 863–886.

O'Connell, R.J. & Budiansky, B., 1978. Measures of dissipation in viscoelastic media, *Geophys. Res. Lett.,* **5,** 5–8.

O'Doherty, R.F. & Anstey, N.A., 1971. Reflections on amplitudes, *Geophys. Prospect.,* **19,** 430–458.

Pointer, T., Liu, E. & Hudson, J.A., 2000. Seismic wave propagation in cracked porous media, *Geophys. J. Int.,* **142,** 199–231.

Pride, S.R., Berryman, J.G. & Harris, J.M., 2004. Seismic attenuation due to wave-induced flow, *J. geophys. Res.,* **109**(B1) art. No. B01201.

Pride, S.R., Tromeur, E. & Berryman, J.G., 2002. Biot slow-wave effects in stratified rock, *Geophysics,* **76,** 271–281.

Rapoport, M.B., Rapoport, L.I. & Ryjkov, V.I., 2004. Direct detection of oil and gas fields based on seismic inelasticity effect, *The Leading Edge,* **23,** 276–278.

Rutherford, S.R. & Williams, R.H., 1989. Amplitude-versus-offset variations in gas sands, *Geophysics,* **54,** 680–688.

Samec, P. & Blangy, J.P., 1992. Viscoelastic attenuation, anisotropy and AVO, *Geophysics,* **57,** 441–450.

Sams, M.S., Neep, J.P., Worthington, M.H. & King, M.S., 1997. The measurement of velocity dispersion and frequency-dependent intrinsic attenuation in sedimentary rocks, *Geophysics,* **62,** 1456–1464.

Shapiro, S.A. & Zien, H., 1993. The O'Doherty-Anstey formula and localization of seismic waves, *Geophysics,* **58,** 736–740.

Shen, F., Sierra, J., Burns, D.R. & Toksoz, M.N., 2002. Azimuthal offset-dependent attributes applied to fracture detection in a carbonate reservoir, *Geophysics,* **67,** 355–364.

Taner, M.T., Koehler, F. & Sheriff, R.E., 1979. Complex seismic trace analysis, *Geophysics,* **44,** 1041–1063.

Taylor, D.B., 1990. *The ANISEIS manual*, Macroc Ltd., Edinburgh, UK.

Tod, S.R., 2001. The effects on seismic waves of interconnected nearly aligned cracks, *Geophys. J. Int.,* **146,** 249–263.

van der Baan, M., 2001. Acoustic wave propagation in one-dimensional random media: the wave localization approach, *Geophys. J. Int.,* **145,** 631–646.

van der Kolk, C.M., Guest, W.S. & Potters, J.H.H.M., 2001. The 3D shear experiment over Natih field in Oman: the effect of fracture-filling fluids on shear propagation, *Geophys. Prospect.,* **49,** 179–197.

Wang, Y.H., Worthington, M.H. & Pratt, R.G., 2002. Decomposition of structural amplitude effect and AVO attributes. Application to a gas-water contact, *Pure appl. Geophysics,* **159,** 1305–1320.

Werner, U. & Shapiro, S.A., 1998. Intrinsic anisotropy and thin multilayering—two anisotropy effects combined, *Geophys. J. Int.,* **132,** 363–373.

White, J.E., 1975. Computed seismic wave speeds and attenuation in rocks with partial gas saturation, *Geophysics,* **40,** 224–232.

White, R.E., 1992. The accuracy of estimating Q from seismic data. *Geophysics,* **57,** 1508–1511.
Worthington, M.H. & Hudson, J.A., 2000. Fault properties from seismic Q, *Geophys. J. Int.,* **143,** 937–944.
Wyllie, M.R., Gregory, A.R. & Gardner, L.W., 1956. Elastic wave velocities in heterogeneous and porous media, *Geophysics,* **21,** 41–70.
Xu, S. & White, R.E., 1996. A physical model for shear-wave velocity prediction, *Geophys. Prospect.,* **44,** 687–717.

APPENDIX A: CALCULATION OF THE FREQUENCY DEPENDENT ELASTIC TENSOR

In this section we outline the procedure for calculating the frequency dependent elastic constants on which our modelling scheme depends. The equations are based on those of Chapman *et al.* (2002), under the simplifying assumption that we consider local ('squirt') flow rather than a combination of local and global flow. In this way we consider frequency dependent wave-induced exchange of fluid between cracks and pores as well as between cracks of different orientations. Cracks are considered to be oblate spheroids ('penny shaped') of low aspect ratio, and the pores are considered to be spherical. The calculations are based on those of Eshelby (1957).

The inputs to the model are the isotropic elastic moduli λ and μ, which in principle are associated with the rock without cracks or pores, the porosity ϕ, a timescale parameter τ, a crack density ε, the crack aspect ratio r and the fluid bulk modulus κ_f. All other parameters being equal, ε controls the magnitude of dispersion and attenuation, while τ controls the frequency range over which that dispersion occurs. Theoretically, τ is proportional to fluid viscosity and inversely proportional to permeability, although there is also a scale dependence (Chapman 2003). τ According to the model, variations in permeability should be modelled by changing the τ value.

To calculate the frequency dependent elastic tensor, we first define the pore- and crack-space compressibility parameters:

$$K_p = \frac{4\mu}{3\kappa_f}; \tag{A1}$$

$$K_c = \frac{\pi\mu(\lambda+\mu)r}{\kappa_f(\lambda+2\mu)}. \tag{A2}$$

We then define non-dimensional parameters:

$$\gamma = \frac{3\pi(\lambda+\mu)}{4(\lambda+2\mu)}\frac{(1+K_p)}{(1+K_c)}; \tag{A3}$$

$$\gamma' = \gamma\frac{\lambda+2\mu}{3\lambda+2\mu}\frac{1}{1+K_p}; \tag{A4}$$

and the frequency-dependent constants:

$$A(\omega) = \frac{(1+i\omega\gamma\tau)\frac{\lambda+2\mu}{(\lambda+\mu)}\left(\frac{16\varepsilon}{27\phi(1+K_p)}+\frac{(\lambda+\mu)}{3\lambda+2\mu}\right)+i\omega\tau\left(\frac{1}{3(1+K_c)}-\gamma'\right)}{1+i\omega\tau+(1+i\omega\gamma\tau)\frac{16\varepsilon(1+K_c)}{9\phi(1+K_p)}\frac{\lambda+2\mu}{(\lambda+\mu)}}; \tag{A5}$$

$$B(\omega) = \frac{\frac{1}{3(1+K_c)}+\frac{9(1+K_p)}{16(1+K_c)}\frac{(\lambda+\mu)}{3\lambda+2\mu}+\frac{i\omega\tau}{1+i\omega\tau}\left(\gamma'-\frac{1}{3(1+K_c)}\right)}{\frac{9(1+K_p)}{16(1+K_c)}\frac{(\lambda+\mu)}{(\lambda+2\mu)}+\frac{1+i\omega\gamma\tau}{1+i\omega\tau}}. \tag{A6}$$

The effective, frequency-dependent, bulk modulus is then given by:

$$\kappa_{\text{eff}} = \kappa - \varepsilon\left[\frac{4(3\lambda+2\mu)(\lambda+2\mu)}{\mu(\lambda+\mu)}\{1-3A(\omega)\}-4\pi A(\omega)r\right] - \phi\left[\frac{(3\lambda+2\mu)}{4\mu}\left\{\frac{\lambda+2\mu}{3\lambda+2\mu}+B(\omega)\right\}-3B(\omega)\right]. \tag{A7}$$

The effective shear modulus is given by:

$$\mu_{\text{eff}} = \mu - \frac{16}{45}\varepsilon\frac{1}{1+K_c}\frac{\mu(\lambda+2\mu)}{3\lambda+4\mu}\left(K_c+\frac{1}{1+i\omega\tau}\right) - \frac{32}{45}\varepsilon\frac{\mu(\lambda+2\mu)}{3\lambda+4\mu}-\phi\frac{15\mu(\lambda+2\mu)}{9\lambda+14\mu}. \tag{A8}$$

Following O'Connell & Budiansky (1978), we define the quality factor Q for P- and S waves, respectively, as:

$$Q_p = \frac{-\text{Re}\left(\kappa_{\text{eff}}+\frac{4}{3}\mu_{\text{eff}}\right)}{\text{Im}\left(\kappa_{\text{eff}}+\frac{4}{3}\mu_{\text{eff}}\right)}; \tag{A9}$$

$$Q_s = \frac{-\text{Re}(\mu_{\text{eff}})}{\text{Im}(\mu_{\text{eff}})}. \tag{A10}$$